Analysis of the Effects of Pulsations on the Operational Stability of Centrifugal Compressors in Mixed Reciprocating and Centrifugal Compressor Stations

Klaus Brun
Southwest Research Institute,
Mechanical and Materials Engineering Division,
P.O. Drawer 28510,
San Antonio, TX 78228-0510
e-mail: kbrun@swri.org

Rainer Kurz
Solar Turbines, Inc.,
9330 Sky Park Court,
San Diego, CA 92123-5398
e-mail: kurz_rainer_x@solarturbines.com

Mixed operation with both centrifugal and reciprocating compressors in a compression plant poses significant operational challenges as pressure pulsations and machine mismatches lead to centrifugal compressors' instabilities or poor performance. Arrangements with reciprocating compressors placed in series with centrifugal compressors generally lead to higher suction/discharge pulsations on the centrifugal compressor than conventional parallel operation. This paper demonstrates that by properly analyzing and designing the interconnecting piping between the compressors, utilizing pulsation attenuation devices, and matching the compressors' volumetric-flow rates, a satisfactory functional compression system design can be achieved for even the worst cases of mixed centrifugal and reciprocating compressor operation. However, even small analysis errors, design deviations, or machine mismatches result in a severely limited (or even inoperable) compression system. Also, pulsation attenuation often leads to a significant pressure loss in the interconnect piping system. Utilizing analysis tools in the design process that can accurately model the transient fluid dynamics of the piping system, the pulsation attenuation devices, and the compressor machine behaviors is critical to avoid potentially costly design mistakes and minimize pressured losses. This paper presents the methodology and examples of such an analysis using a 1D transient Navier–Stokes code for complex compression piping networks. The code development, application, and example results for a set of mixed operational cases are discussed. This code serves as a design tool to avoid critical piping layout and compressor matching mistakes early in the compressor station design process. [DOI: 10.1115/1.4000299]

1 Introduction

The mixed operation of centrifugal and reciprocating compressors in a single compression plant has become common design practice over the past 20 years as this arrangement can provide some benefits for highly cyclical process profiles. In many of theses stations, the compressors are placed in parallel operation such that large gas turbine driven centrifugal compressors provide the base-load compression while smaller reciprocating compressors follow cyclical or peaking demand compression demands. In these cases, the centrifugal compressors may experience some pulsations from the reciprocating compressors on both the common suction and discharge headers, but good reciprocating compressor bottle and manifold designs usually result in minimal impact on the operational stability of the centrifugal compressors.

However, some recent designs have reciprocating compressors placed in series with centrifugal compressors for either high pressure ratio applications or to take advantage of the operational flexibility of a centrifugal compressor (i.e., both arrangements with the reciprocating compressor upstream and downstream of the centrifugal compressor are proposed). For example, a centrifugal compressor may be placed upstream of a reciprocating compressor in gas-reinjection applications to handle the higher flow volumes at low pressure while the reciprocating compressors are better equipped for high pressures and pressure ratios.

On the other hand, centrifugal compressors are often installed downstream of one or multiple reciprocating compressors in gas gathering applications where multiple, very low pressure streams from the reciprocating compressor(s) are combined into one larger volume medium pressure stream to be compressed to pipeline pressure by the centrifugal compressor. These plant arrangements can lead to significantly higher relative pulsations on the centrifugal compressor than parallel operation, and the operational stability of the compressor may be affected. Typically, a centrifugal compressor operating with a suction pressure of 40 bars (600 psi) and discharge pressure of 70 bars (1000 psi) may experience upstream pulsations from a reciprocating compressor exceeding 10 bars (150 psi) peak-to-peak, if no pulsation attenuation devices (bottles, choke tube, or orifice plates) are utilized or an acoustic pipe resonance exists. These suction pressure variations of up to 25% will clearly present a challenge for any centrifugal compressor aerodynamic stability, especially if the compressor operates near its surge line. Thus, the piping arrangement between reciprocating and centrifugal compressors must be properly analyzed to avoid acoustic resonance conditions and/or attenuate the pressure pulsations from the reciprocating compressor.

A methodology and examples of such an analysis are presented herein. To properly model the highly pulsating pipe flow, a full 1D transient Navier–Stokes code was developed for any piping net-

Contributed by the International Gas Turbine Institute (IGTI) of ASME for publication in the JOURNAL OF ENGINEERING FOR GAS TURBINES AND POWER. Manuscript received June 10, 2009; final manuscript revised July 14, 2009; published online April 21, 2010. Editor: Dilip R. Ballal.

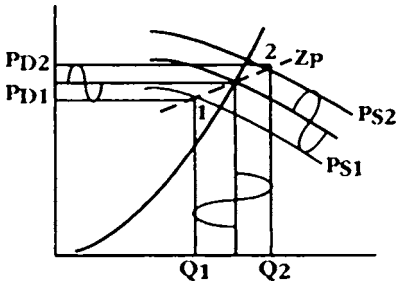

Fig. 1 Pulsation transmission in centrifugal compressors [17]

work matrix. Boundary condition pulsations are generated by a reciprocating compressor cylinder model and a simple centrifugal compressor flow interface. The resulting total impact of the combined pulsation, including the effects of pipe resonant conditions, was imposed on the centrifugal operating map as either suction or discharge pressure fluctuations to determine the effect on the operational stability of the compressor. Example results on centrifugal compressor performance impact, surge margin, and choke limits, and other operational margins are discussed below.

2 Background

Classical pulsating flow compressor manifold and piping design involves optimum selection and use of primary volumes, choke tubes, and secondary volumes, as well as cylinder phase cancellation. These elements are used in designing pulsation filters that provide a sufficient volume for the high unsteady flow entering and leaving the compressor cylinders. While providing sufficient volume to filter the unsteady flow pulsations from the compressor, these filters must also be designed to avoid excitation of "acoustic" resonance inherent to the installation piping and in the compressor station filter system [16]. However, even well-designed pulsation dampeners for reciprocating compressors allow low frequency pressure pulsations in the range of one to several percent of the operating pressure to enter the piping system [13].

A centrifugal compressor either attenuates or amplifies pulsations at its discharge or suction side, because it reacts to any fluctuation in flow with a fluctuation in head and, thus, pressure ratio, which can be easily seen from its performance characteristic in Fig. 1 [17]. Especially for very slow fluctuations (less than 1 Hz), the process control system, in the attempt to keep the suction or discharge pressure constant, may cause problems by cycling the power generated by the gas turbine, and subsequently the speed of the compressor.

Sparks [17] explained the process as the interaction of a piping system with given acoustic impedance and a compressor that reacts to a change in flow with a change in head (or pressure ratio). The piping impedance is usually a combination of resistive impedance (i.e., due to frictional losses) and acoustic inertia (due to the mass of the gas in the pipe) and stiffness (due to the compressibility of the mass in the pipe). The compressor head-flow characteristic will exceedingly differ from the steady-state characteristic for higher fluctuation frequencies. Sparks [17] also discussed practical piping system design approaches to reduce pulsation levels using acoustic elements, such as bottles, nozzles, choke tubes, and resonators.

A number of other studies are available in the public domain that evaluates the impact of flow pulsations on turbomachines. A detailed literature review on this topic was provided by Kurz et al. [13], and an overview of the state-of-the-art of pulsation analysis technologies was included in Ref. [6], and thus, these studies are not further discussed herein. However, relevant references are provided for completeness [1–20].

3 Rationale

In the past, for low-speed reciprocating gas compressors, acoustic (pressure) pulsation, and mechanical resonance avoidance was used to sufficiently control pulsation and vibration levels at a gas compressor station. To determine the acoustic resonance frequencies, solvers of the transient acoustic wave equations were utilized, which have been demonstrated to provide, in most cases, accurate results for compression system resonance frequencies and reasonable agreement for pulsation amplitudes. However, the mathematical assumptions associated with solving the acoustic linearized wave equations must lead to discrepancies in amplitude predictions, as these equations are only a partial physical model of the actual transient fluid dynamics. Furthermore, inherently any acoustic wave model in the frequency domain cannot accurately predict steady and transient pressure drops, as no bulk flow is modeled. Especially for modern variable speed high-speed reciprocating compression systems, where complete resonance avoidance is often impossible, accurate prediction of pressure amplitudes is critical to allow for proper structural pipe and pipe support design. Unfortunately, for these cases, both frequency and amplitude predictions of pressures have been demonstrated to be inaccurate [6].

A full one-dimensional representation of the governing transient fluid dynamic equations (the Navier–Stokes equations) can provide a more thorough solution for the pulsating flow field and can provide more accurate pulsation amplitude predictions. This is particularly critical in the design of piping systems between variable high-speed reciprocating compressors and centrifugal compressors, as the centrifugal compressor stability is sensitive to highly pulsating flows [13] and as operating at resonance frequencies cannot usually be avoided.

When a centrifugal and a reciprocating compressor are interfaced within the same piping system, there are principally three transient fluid mechanisms that have the potential to create damaging inlet/outlet conditions on the centrifugal compressor. These mechanisms are as follows:

1. pulsations generated by the reciprocating compressor
2. pulsations generated by the reciprocating compressor that are amplified by an acoustic resonance within the piping system
3. a mismatch between the operating points of the centrifugal and reciprocating compressors causing the machines to continuously "hunt" for a stable operating point

All of these mechanisms can move the centrifugal compressor operating point into a surge or choke (stonewall) condition and, thus, should be avoided or at least controlled. Pulsation mechanisms 1 and 2 can be mostly analyzed using a basic (classic) acoustic pulsation model (transient wave equation) of the piping system. However, the analysis of transient flow created by an operating unbalance between the compressors (mechanism 3) requires a "true" transient flow solver that fully models flow density and pressure changes and also properly models the physical (thermodynamic) function of compressors. The operational unbalance is created by the fact that for a given running speed a reciprocating compressor is effectively a constant volume-flow machine (with only a small range depending on the compressor's clearance volume), whereas a centrifugal compressor is controlled by fixed head-flow relationship. Any mismatch in volume flow between the compressors will create a pressure imbalance that moves the operating point of both centrifugal and reciprocating compressors. In most cases, this results in continuous low frequency pressure fluctuations that are not necessarily periodic. This fluctuation is a complex function of the operating condition, compressor designs, and the interconnecting piping geometry. The analysis is often further complicated by the control system of the centrifugal compressor, which is designed to vary the speed of the compressor to

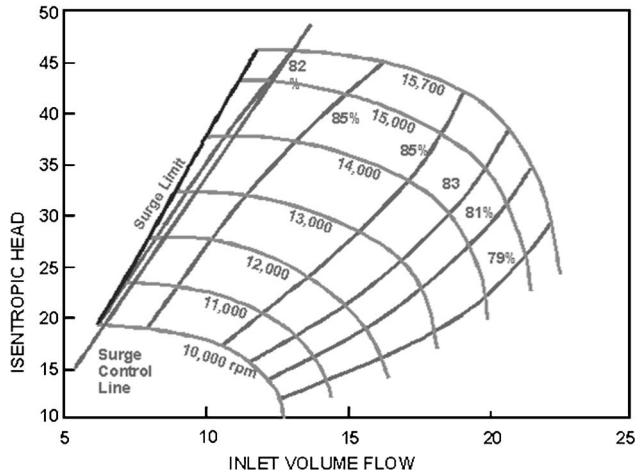

Fig. 2 Typical compressor map for boundary condition

maintain either a constant discharge or suction pressure. A continuous nonperiodic cycling of the centrifugal compressor speed is often the result.

Obviously, for this type of analysis, any "linearized" solutions of the transient wave equation or even transient perturbation transport solutions, such as those employing the method of characteristics or finite wave methods, are inherently not suitable, as they do not fully model the fluid flow and compressor physics. Thus, a full solution of the Navier–Stokes equation coupled with physical compressor models is the most appropriate solver to model the transient fluid flow and interaction of interconnected reciprocating and centrifugal compressors.

4 Analysis Model

A full one-dimensional time-domain flow solver applicable to any complex interconnected manifold and piping system was developed to determine the highly transient fluid pulsations in mixed reciprocating and centrifugal compressor stations. This transient flow solver included all terms of the governing equations, including fluid inertia, diffusion, viscosity, and energy dissipation. Physical models for both centrifugal and reciprocating compressors were also derived and implemented into the solver.

4.1 Compressor Models. The state of the gas in any compressor manifold and attached piping system is determined by two factors: (1) the kinematics of the compressor drive, which provides a forcing inlet boundary condition to the piping system, and (2) the fluid dynamic behavior (response) of the piping system and all outlet boundary condition. A reciprocating compressor cylinder boundary condition is determined from its piston position, $z(\varphi)$, which is given by

$$z(\varphi) = \frac{V_s}{A_P} + r \times (1 - \cos\varphi) + \frac{r}{\lambda} \times (1 - \sqrt{1 - \lambda^2 \sin^2\varphi}) \quad (1)$$

and the cylinder valve positions, which is a function of the cylinder internal pressure. For a centrifugal compressor, boundary conditions can be derived directly from a specific compressor performance map as shown in Fig. 2. This map must be obtained from the centrifugal compressor manufacturer or from test data. For numerical simplicity, this map can often be further simplified by nondimensionalizing the flow and head into characteristic psi-phi [15] curves. However, given the very short period of flow transients (in the order of 0.5–100 Hz) and the significant rotational inertia of a gas turbine driven centrifugal compressor, it is accurate to model the centrifugal compressor as a constant speed machine. This assumption can be validated for a given application by calculating a nondimensional parameter that ratios pulsating aerodynamic torque on the impeller with the rotor's total angular inertia. The authors derived (and have successfully utilized) the following nondimensional (Brun–Kurz) number C for this analysis:

$$C = \frac{\omega r^2 \Delta\dot{m}}{(2\pi) J f^2} \quad (2)$$

where $\Delta\dot{m}$ is the inlet mass-flow pulsation peak-to-peak magnitude, ω is the angular speed of the centrifugal compressor (in rad/s), r is the tip radius of the centrifugal compressor impeller, J is the moment of inertia of the rotor, and f is the pulsation frequency (in hertz). For small values of the Brun–Kurz number C, the inertial forces dominate the pulsating aerodynamically induced torque, and one can assume that the impeller speed remains constant and unaffected by pulsations. This simplifies the centrifugal compressor boundary condition to a simple second order polynomial

$$H = \Gamma_1 + \Gamma_2 Q + \Gamma_3 Q^2 \quad (3)$$

where the coefficients are determined from the compressor map. A parabola was used herein but for some applications higher order polynomials can provide a better representation of the compressor map. The limits of this polynomial are surge on the low flow side and choke on the high flow side. Thus, for a given compressor speed, Eq. (3) and the fan law are utilized to obtain flow for a given pressure suction and discharge condition.

4.2 Governing Equations. A thorough description of the governing equations of one-dimensional transient flow was provided by Morini et al. [21], and, thus, the derivation is only briefly reviewed. Collectively, the continuity, momentum, and energy equation generalized for compressible Newtonian fluids (the Navier–Stokes equations) govern compressible fluid flow in a compressor manifold system. In order to solve for pressure and velocity in one dimension, the momentum and continuity equations may be used in combination with an equation-of-state. These equations provide three independent solutions for three unknowns (usually pressure, density, and velocity).

The transient 1D momentum equation (without the influence of body forces, such as gravity) is expressed as

$$\frac{\partial(\rho u)}{\partial t} + u\frac{\partial(\rho u)}{\partial x} + \frac{\partial P}{\partial x} = \mu\left(\frac{\partial^2 u}{\partial x^2} + \frac{\partial^2 u}{\partial y^2}\right) \quad (4)$$

The continuity equation is

$$\frac{\partial \rho}{\partial t} + \frac{\partial(\rho u)}{\partial x} = 0 \quad (5)$$

In the above momentum equation, the viscosity μ in the streamwise (x) direction is the combined viscosity and turbulent eddy viscosity, where the turbulent eddy viscosity is usually determined using a second order Reynolds number based turbulence model. The second viscous loss term can simply be treated as a pipe friction loss f.

$$f = \mu\left(\frac{\partial^2 u}{\partial y^2}\right) = \frac{1}{2}\rho u^2 k \quad (6)$$

The friction factor k is obtained from empirical models (e.g., Moody diagram). Note that the energy equation is not included here as it can be solved as a simple algebraic pressure loss equation.

The turbulence eddy viscosity is handled explicitly and is determined from a second order Reynolds number turbulence model. In-pipe flow, there are two terms in the momentum equation that include viscosity: (a) the second partial derivative in the streamwise direction, and (b) the second partial derivative in the streamnormal direction. The (b) term can be treated implicitly using a basic pipe friction loss coefficient and does not require viscosity directly (only within the context of Reynolds number). The (a) term does require viscosity (and turbulence eddy viscosity) directly and must be handled explicitly. To properly capture the

nonlinearity of this term, small time-steps and fine grid spacing are required. However, as this time-step and grid spacing are not smaller than what is required to capture complex wave shapes of high frequency pulsating flow, this was not found to be a limitation.

Thus, the transient inviscid momentum equation is

$$\rho\frac{\partial u}{\partial t}+\rho u\frac{\partial u}{\partial x}+\frac{\partial P}{\partial x}=0 \tag{7}$$

Note that the viscosity term was eliminated in the above equation (i.e., these equations are effectively Euler equations). However, the viscosity and pressure (energy) loss terms are not neglected, but rather are explicitly treated at every time-step and used to correct pressures and velocities at all nodes.

In order to account for changes in area in the system, area must be included in the continuity equation. Area may be regarded as constant with respect to time and space, and as such, it may be brought inside the derivative.

$$\frac{\partial(\rho A)}{\partial t}+\frac{\partial(A\rho u)}{\partial x}=0 \tag{8}$$

The momentum equation can be rewritten as

$$\frac{\partial}{\partial t}(\rho u)+\frac{\partial}{\partial x}(\rho u^2+P)=0 \tag{9}$$

For acoustic applications, the speed of sound c is substituted for density as the speed of sound can be directly determined from the equation-of-state

$$c^2=\left(\frac{\partial P}{\partial \rho}\right) \tag{10}$$

which can also be written as

$$c=\sqrt{\frac{\gamma p}{\rho}} \tag{11}$$

for a real gas. Thus, the final equations to be written are

$$\frac{\partial}{\partial t}\left(\frac{PA\gamma}{c^2}\right)+\frac{\partial}{\partial x}\left[\frac{PA\gamma u}{c^2}\right]=0 \tag{12}$$

$$\frac{\partial}{\partial t}\left[\frac{P\gamma u}{c^2}\right]+\frac{\partial}{\partial x}[P\gamma m^2+P]=0 \tag{13}$$

4.3 Numerical Method. The Lax–Wendroff method was selected for speed and stability as the most appropriate numerical approach to solve the above equations. As this method is well described in literature [8], it is only briefly outlined herein. The LW2 method uses a basic forward time and centered space numerical approximation as a first step, but requires finding an intermediate time solution at $t=*$ and an intermediate space solution at $x=j+1/2$. A centered space and forward time scheme is applied at the intermediate time-step in the second step equation to derive the final spatial and time derivatives.

The momentum and continuity equations shown above can be expressed in the following form for the numerical approximation scheme:

$$\frac{\partial\vec{q}}{dt}+\frac{\partial\vec{F}}{\partial x}=0 \tag{14}$$

where q and F are vectors

$$q=\begin{bmatrix}\frac{PA\gamma}{c^2}\\ \frac{P\gamma u}{c^2}\end{bmatrix}F=\begin{bmatrix}\frac{PA\gamma u}{c^2}\\ P(1+m^2\gamma)\end{bmatrix} \tag{15}$$

As previously noted, here the energy equation and viscosity are decoupled and treated explicitly in between time-steps to enhance computational efficiency. This results in a two-equation model with the requirement for relatively small time-steps but a time-space step dependency. The viscous energy loss terms can be divided into pipe friction loss and through-flow viscous energy dissipation; both terms are separately calculated and applied at all nodes. One should note that the viscous through-flow energy dissipation represents the velocity gradient losses in the pipe flow direction, which is usually very small for steady flow but can be significant for pulsating flows. The conventional pipe friction loss must also be included, as it accounts for the normal flow gradient viscous losses, which are primarily steady-state effects.

Within this project, a three-equation model (with the energy equation coupled) was also developed and compared with the two-equation model; as differences were found to be negligible, only the two-equation model was further advanced. One should note that the energy losses of the system are effectively pressure drops (and can be obtained from well-established empirical pipe friction formulations), whereas the viscosity term results in an enthalpy reduction that must be converted to a pressure drop to be useful in the above model.

Unless a cooler is utilized, measurements at many stations have shown that gas temperature drops between compressor discharge and station exit are less than 0.5°C because of the dominant convection heat transfer from the process gas. Even at very low ambient conditions, the gas temperatures throughout compressor stations tend to be constant and, thus, the influence of heat transfer on the pulsation can be neglected. Nonetheless, the model does allow for gas temperature changes, but they are included in the model in the form of gas property changes from the real equation-of-state of the particular gas mixture (no ideal gas assumption) rather than heat transfer in the energy equation.

4.4 Equation Discretization. The spatial derivative is solved at every $\frac{1}{2}$-step using the following equation to yield an intermediate transient derivative at time=*:

$$\left[\frac{\partial q}{\partial t}\right]^*_{j+1/2}=-\left[\frac{\partial F}{\partial x}\right]^n_{j+1/2} \tag{16}$$

In discretized form, using a forward time and centered space method, the above derivatives become

$$\frac{q^*_{j+1/2}-q^n_{j+1/2}}{0.5\Delta t}=-\left[\frac{F^n_{j+1}-F^n_j}{\Delta x}\right] \tag{17}$$

The time derivative is solved for the intermediate time-step.

A linear relationship is assumed to exist q_j and q_{j+1}, and a weighted value based on the physical length of Δx_{j-1} and Δx_j is used to estimate q at $j+1/2$ for $t=n$ as follows:

$$q^n_{j+1/2}=q^n_j+(q^n_{j+1}-q^n_j)\cdot W_i \tag{18}$$

where

$$W_i=\text{weighting factor}=\frac{\Delta x_{j-1}}{(\Delta x_{j-1}+\Delta x_j)} \tag{19}$$

the resultant equation for the first time-step is

$$q^*_{j+1/2}=-\frac{0.5\Delta t\cdot(F^n_{j+1}-F^n_j)}{\Delta x}+0.5\cdot(q^n_{j+1}+q^n_j) \tag{20}$$

For the second time-step, the governing equation is applied to provide the final q values at $x=j$ and $t=n+1$, namely,

$$\left[\frac{\partial q}{\partial t}\right]^{n+1}_j=-\left[\frac{\partial F}{\partial x}\right]^*_j \tag{21}$$

The discretized version of the second step-time equation, using a forward time and centered space scheme, results as follows:

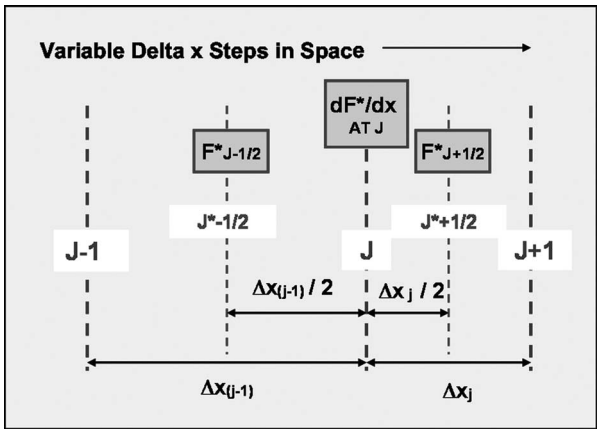

Fig. 3 Lax–Wendroff discretization

$$q_j^{n+1} = q_j^n - \frac{\Delta t}{(0.5\Delta x_{j-1} + 0.5\Delta x_j)} \cdot [F^*_{j+1/2} - F^*_{j-1/2}] = q_j^n - \frac{2\Delta t}{(\Delta x_{j-1} + \Delta x_j)} \cdot [F^*_{j+1/2} - F^*_{j-1/2}] \tag{22}$$

Figure 3 graphically represents this discretization formulation. The advantages and limitations of the above-described method are discussed by Fletcher [8] and are thus not further discussed herein.

In a complex piping system, the above set of equations must be individually solved for all pipe segments with the appropriate inlet and outlet conditions updated at each time-step. Within each pipe segment, the simple central difference discretization (as described above) and time-space forward marching solution was utilized. Pressure losses inside the pipe and at the interfaces are determined from basic pipe friction loss models, and viscosity losses are directly calculated from the discretized viscosity term of the momentum equation (along the flow direction); these two terms are applied at every time-step at every applicable node. Thus, the viscous terms are not simply treated as a pipe friction loss but also include a discretization of the x viscous term (in the flow direction). The x discretized term and the pipe friction viscous term are calculated for each node after determining the half step $(j+1/2)$ and are then included to determine the full step $(j+1)$. This allows for coupling of the viscous terms with the inertial and pressure terms of the momentum equations.

Pipe inlet and outlet conditions, which are also enforced at every time-step, where either active inlet forced (sinusoid and square wave) or active unforced functions (compressor), pipe intersections (branching nodes), or passive-end conditions (infinite pipe, open- or closed-end).

4.5 Pipe Interfaces. Formulations must be provided to determine boundary conditions at multiple pipe interfaces, such as pipe tees or joints. The continuity equation may be applied to determine the resulting velocity in each pipe inlet and outlet. The two cases are shown below in Figs. 4 and 5.

If two inlet flows (Reaches 0 and 1) combine to provide a final output flow (Reach 2) as in Fig. 4, then the equations for the velocity at the intersection point based on the velocities in each reach can be derived as follows:

$$u^0_{\text{int}} = \frac{u^0_{j-1} \cdot A^0_{j-1}}{A_{\text{int}}} \tag{23}$$

$$u^1_{\text{int}} = \frac{u^1_{j-1} \cdot A^1_{j-1}}{A_{\text{int}}} \tag{24}$$

where

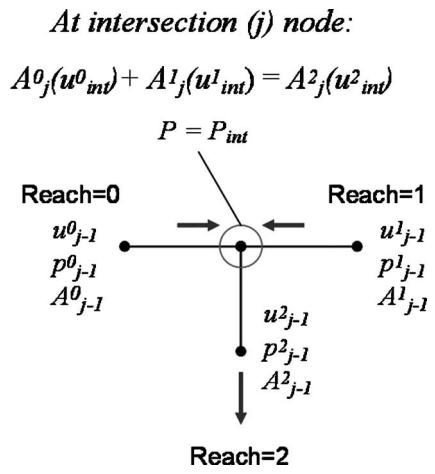

Fig. 4 Branching node intersection (2 inlets/1 outlets)

$$A_{\text{int}} = \frac{(A^0_j + A^1_j + A^2_j)}{3} \tag{25}$$

$$u^2_{\text{int}} = \frac{u^0_{\text{int}} \cdot A^0_j + u^1_{\text{int}} \cdot A^1_j}{A^2_j} \tag{26}$$

The average area of the intersection point is used to solve for the inlet velocity in each reach at the intersection point. Pressure is assumed to be equal at the intersection point at each time-step. The pressure in each reach at the node previous to the reach (i.e., at $(j-1)$ if the intersection point is considered to be j) is used to determine the weighted contribution toward the pressure at the intersection point. The pressure is weighted by multiplying by the area of the reach and its corresponding delta x length. The equation used to determine pressure at the intersection point is given in

$$P_{\text{int}} = \frac{\sum_{n=1}^{3} (P^i_{j-1} \cdot A^i_{j-1})}{\sum_{n=1}^{3} (A^i_{j-1})} \tag{27}$$

Using these equations, the velocity at the intersection point in each reach is based on continuity, and the pressure at the intersection point is based on the weighted average of the pressures in each reach. The interface nodes are actually zero-volume nodes, and, thus, although integral expressions are used, there is no dif-

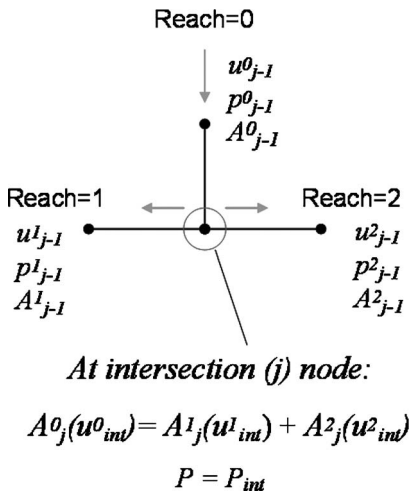

Fig. 5 Branching node intersection (1 inlet/2 outlets)

Table 1 Pipe interface and end-conditions

Active
Compressor cylinder
Centrifugal compressor
Sine wave
Square wave
Passive
Infinite-end
Open-end
Closed-end
Pipe interfaces
1-1 pipes
2-1 pipes
3-1 pipes
Transitions
In-pipe
Orifice plates
Discrete pressure drops

ference between this approach or any differential interface implementation. As the interface pressures and mass-flows are determined from a balance of the surrounding nodes, transient terms of the governing equations are implicitly included.

4.6 End-Conditions. Boundary end-conditions, such as open-ended pipe, closed pipe, or infinite pipe also must be defined but are relatively straightforwardly determined from basic physics. For example, at an open-ended pipe, the interface node pressure is set to ambient while velocity is conserved. Similarly, at a pipe closed-end, the velocity is set to zero and pressure maintained. Inlet conditions can be either forced with a hard boundary condition (sinusoids or square waves) or unforced with a downstream dependent function (compressor cylinders). As compressor cylinders are varying-volume machines, boundary conditions, based on velocity rather than pressure, were found to be more practical and physical to implement. The applicable boundary and interface conditions are shown in Table 1.

4.7 Code Implementation. The unsteady one-dimensional Navier–Stokes code was written for a complex system of pipes with multiple interfaces and has all standard boundary conditions, such as open-ends, closed-ends, a compressor cylinder, sine wave, and square waves, available. Interfaces between pipe segments can be one-on-one, two-on-one, one-on-two, one-on-three, or three-on-one, and include discrete pressure drops at the segment interfaces. Other boundary conditions are either passive (closed wall, open wall, and infinite pipe) or active (compressor, sine wave, and square wave). The pipe areas can change either gradually (transition piece) or abruptly (open-end or bottles) within the pipes or at the interfaces of pipe segments. Models with up to 60 interconnected pipe segments were successfully tested. A Windows file preprocessor, graphical user interface, and graphical postprocessor (for frequency- and time-domain data) were also implemented. Figure 6 shows the user interface for a typical compression station model. Full frequency sweeps can be performed

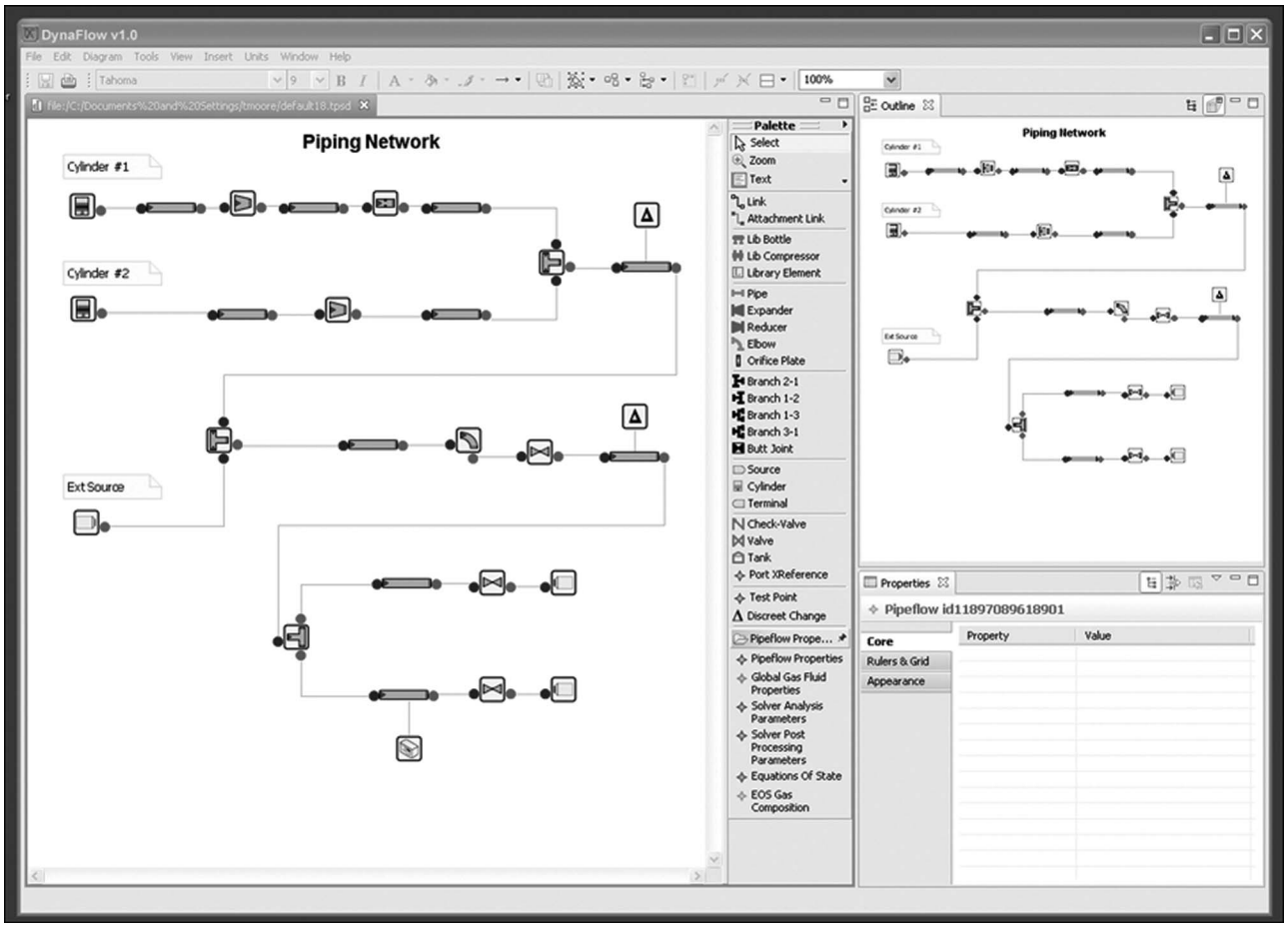

Fig. 6 Graphical user interface for solver

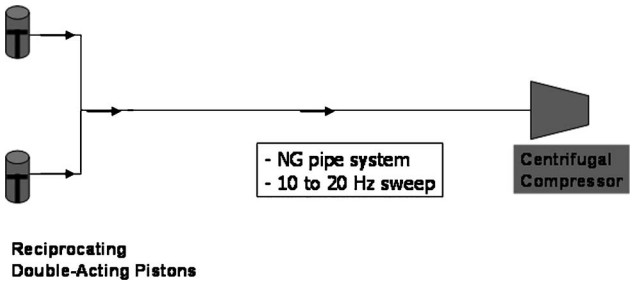

Fig. 7 Case 1—reciprocating compressor upstream of centrifugal compressor

with all boundary conditions. The postprocessor interface includes a Hanning window function, a time domain, and a FFT output option. A detailed validation of the subject code was presented by Brun et al. [6].

5 Case Studies

The above-described software was utilized to determine the transient flow and operation of a set of simple compression systems as shown in Figs. 7–9. These idealized cases were chosen to illustrate the methodology. In these cases, a double-acting reciprocating compressor (two single-ended cylinders at 180 deg out of phase) was mounted 30 m upstream from a centrifugal compressor. Case 1 is a simple straight pipe, while Cases 2 and 3 include pulsation attenuation devices in the pipe system. Namely, Case 2 incorporates a simple orifice (area ratio 1:5) while Case 3 has a bottle with an internal choke tube (bottle area ratio 6:1 and choke tube area ratio 1:4) and also an orifice plate (area ratio 1:5). The fluid in the system is methane at an absolute pressure of 2089 kPa (at the reciprocating compressor discharge), a speed of sound of 444 m/s, and an isentropic coefficient of 1.35. The reciprocating compressor has the following design data:

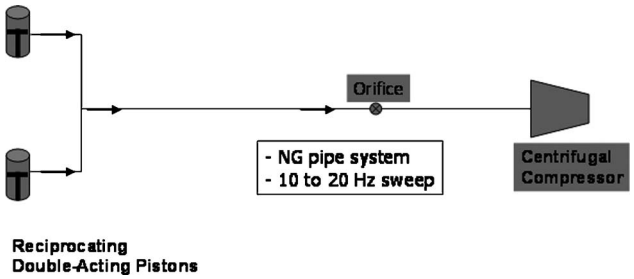

Fig. 8 Case 2—reciprocating compressor upstream of centrifugal compressor with orifice plate

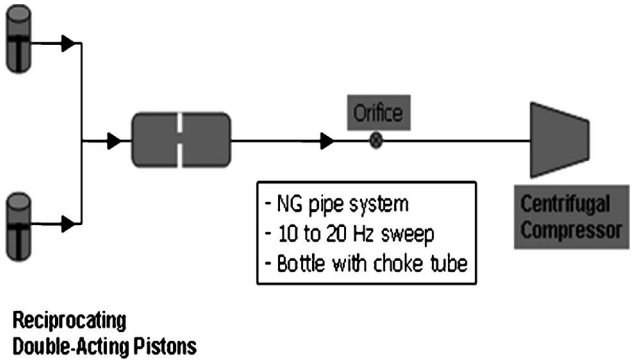

Fig. 9 Case 3—reciprocating compressor upstream of centrifugal compressor with bottle, choke tube, and orifice plate

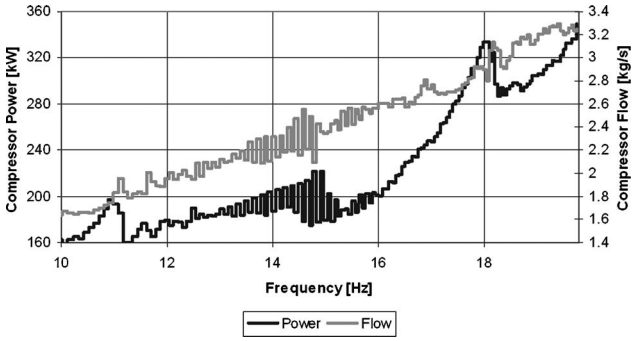

Fig. 10 Reciprocating compressor power required

- stroke: 0.2 m
- bore area: 0.05 m^2
- rod length: 0.5 m
- speed: 10–20 Hz
- pressure ratio: 2.0
- clearance volume: 5% (0.0005 m^2)

The resulting flow ranged between 1.6 kg/s and 3.3 kg/s, and the power (calculated for the compressor p-v curve) ranged between 160 kW and 340 kW, primarily depending on compressor speed. Figure 10 shows the power required and flow produced by the reciprocating compressor over a speed sweep from 10 Hz to 20 Hz. For this example, the centrifugal compressor modeled as operating at the lower end of its head-flow map at a constant speed of 8000 rpm (see Fig. 16 for the head-flow map used). The nondimensional Brun–Kurz number that relates rotor inertia to aerodynamic pulsation torque C_s (described in Eq. (2)) ranges between 0.001 and 0.002 for this case, which indicates that the centrifugal compressor's angular speed will not fluctuate due to the inlet pulsations. To simplify the example further, it is assumed that the compressor operates on constant speed control. Thus, as the reciprocating compressor speed and flow increase, the downstream centrifugal compressor will simply follow its speed line and decrease head until it reaches choke. The surge limit at the 8000 rpm speed is at a minimum flow of 1.7 kg/s and choke is at a minimum pressure ratio of 1.1.

5.1 Compressor Inlet Pulsations. The transient flow field at the compressor inlet is presented in Figs. 11–14. These data can be viewed and analyzed in various forms. For example, Fig. 11 simply shows the compressor inlet velocity as a function of time for Case 2. High velocity fluctuations can be observed, with the compressor inlet flow fluctuations being largest at about 7 s into the speed sweep. Inlet flow velocity pulsations continuously reach negative values between 6 s and 10 s of the sweep. As in this case a 10–20 Hz frequency sweep was performed over a 10 s interval, it can be deduced that the compressor would experience inlet flow reversal (and, thus, immediate surge) at any reciprocating com-

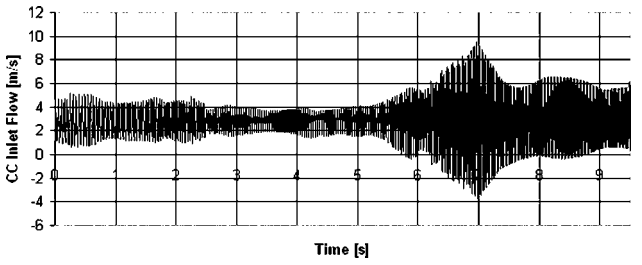

Fig. 11 Case 2—centrifugal compressor inlet velocity versus time

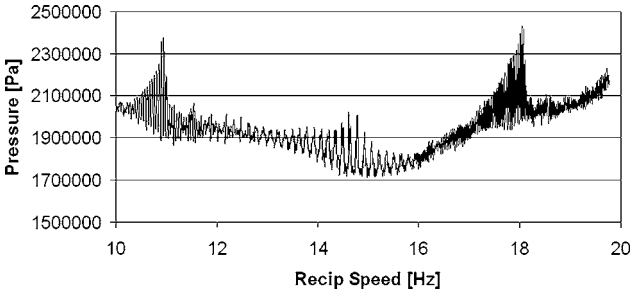

Fig. 12 Case 1—centrifugal compressor inlet pressure fluctuation versus frequency

pressor operating speed above 16 Hz (6 s). Thus, without any further analysis, it becomes apparent that system would not operate as designed over the full speed range.

To perform a more rigorous analysis, it is more convenient to plot pressure versus frequency to determine not just pulsations but also any low frequency total pressure trends. For example, Figs. 12–14 show the compressor inlet pressure as a function of frequency for Cases 1, 2, and 3, respectively. Both Cases 2 and 3 utilize pulsation attenuation devices and, thus, have significantly lower pulsations than Case 1. Peak amplitudes are seen at compressor speeds of 18 Hz, 17 Hz, and 19 Hz for Cases 1, 2, and 3, respectively. Surprisingly, although Case 3 utilizes a bottle, a choke tube, and an orifice, the pulsation amplitude reduction when compared with Case 2 (which only uses an orifice) is not significant. Furthermore, low frequency flow transients are clearly more pronounced for Case 3 than for Case 2. This indicates that the pulsation attenuation for Case 3 is not well designed and that the compressors are not mass-flow matched (as discussed above). When comparing Cases 1, 2, and 3, one should also note that the attenuation devices not only affect the pulsation magnitudes but also result in a pronounced resonance frequency shift.

Figure 15 shows the inlet pressure pulsations when converted to the frequency domain (using a fast Fourier transform). The plot compares the peak-hold pressures in the frequency domain to determine all critical system resonance frequencies excited by the reciprocating compressor over its design operating range. The frequency-domain results show that, except for Case 1 where high first order pulsations are in the 10–20 Hz range, the majority of peak-to-peak pulsations for Cases 2 and 3 are second order synchronous. This type of system response is relatively common for double-acting reciprocating piston cylinders on a common and well-balanced header. Case 1 shows a strong first order resonance at 11 Hz and then equally strong second and third order resonances at 22 and 33 Hz. For Case 2, the first order response was filtered by the orifice, but weak second and third order responses are still evident. As previously noted, the addition of a bottle and choke tube for Case 3 did not provide significant additional pulsation damping but shifted resonance frequencies to above 26 Hz (second order) and 39 Hz (third order). Shifting resonance frequencies away from a desired operating speed is a useful feature of bottle-choke-tube combinations and is commonly used in piping pulsation design.

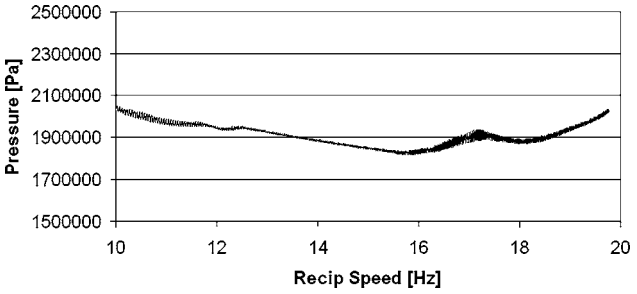

Fig. 13 Case 2—centrifugal compressor inlet pressure fluctuation versus frequency

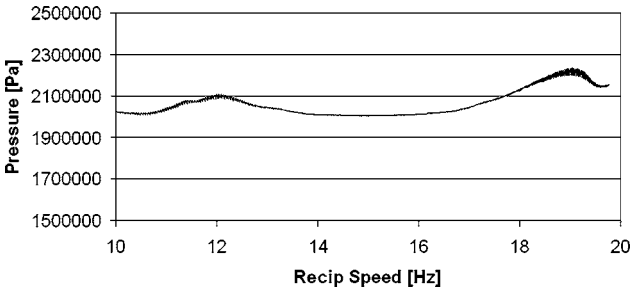

Fig. 14 Case 3—centrifugal compressor inlet pressure fluctuation versus frequency

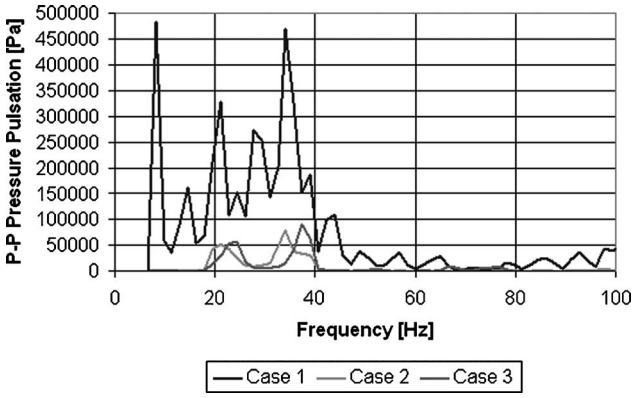

Fig. 15 Cases 1, 2, and 3 pulsation spectrum

5.2 Piping System Head Losses. Obviously, when designing a compression station piping system, the total pressure drop across the piping system is the most critical design objective, once flow stability is assured. A well-designed interconnect piping should have minimum pressure losses while providing adequate pulsation damping to avoid damaging the machinery and piping. Unfortunately, acoustic attenuation devices, such as orifice plates, bottles, and choke tubes, have inherently high pressure losses. For example, Table 2 shows the pressure drop across the piping systems for the above Cases 1, 2, and 3. Table 2 also demonstrates the total power of the reciprocating compressor that is lost due to these pressure drops.

Clearly, the attenuation devices in Cases 2 and 3 are the cause for significant flow head losses and, thus, total system efficiency. For Case 3, nearly 3.1% of the power to compress the gas is lost for pulsation attenuation in the downstream piping.

5.3 Impact on Centrifugal Compressor. As previously noted, for modeling purposes, it is acceptable to assume that the relatively fast flow transients experienced by the centrifugal compressor do not affect the compressor's operational speed. The centrifugal compressor continues to operate at a constant speed as the rotational inertia of the compressor (and power turbine) will tor-

Table 2 Interconnect pipe pressure losses

Case	Pressure loss (Pa)	Power loss (%)
1 (straight pipe)	200	0.0
2 (pipe, orifice)	26,000	2.5
3 (pipe, bottle, choke tube, orifice)	32,000	3.1

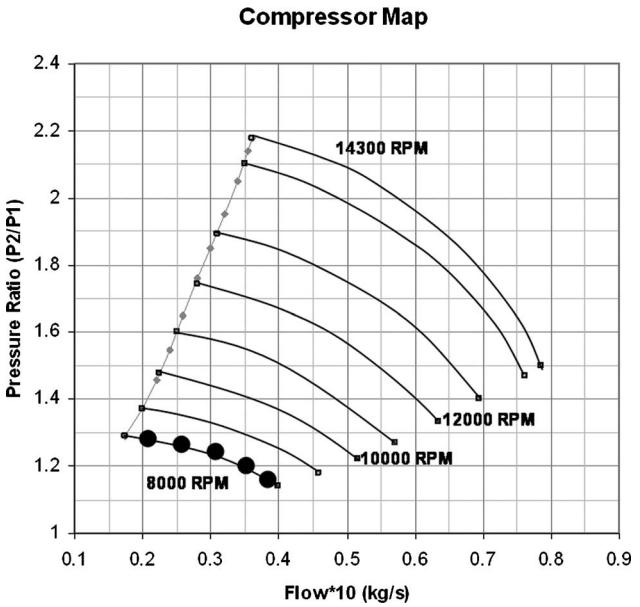

Fig. 16 Operating range of centrifugal compressor due to inlet pulsations

sionally dampen any fluid induced by the rapid blade loading changes. Thus, the compressor will operate on a fixed head-flow speed line, which is limited by surge on the low flow/high pressure and choke on the high flow/low pressure side. As previously noted, this curve can be functionally expressed by Eq. (3).

Although choke should be avoided, as it is an inefficient operating regime, it is not necessarily damaging to the compressor. On the other hand, it is critical to avoid any kind of surge event, as these can cause bearing or seal damage, blade rubbing, or even catastrophic compressor failures. The surge limit of the compressor at a given speed is usually defined by a flow limit, whereas choke is defined by a minim head. Strong pulsations in pressure and flow have the capability to move a centrifugal compressor into surge or choke. For example, Fig. 11 (Case 2) above clearly showed that the centrifugal compressor would experience very low and even negative inlet flows for short periodic time intervals when the upstream reciprocating compressor runs at any speed above 16 Hz (960 rpm). In this case, a strong pulsation second order harmonic at 33 Hz is evident in Fig. 15. Thus, the time intervals of significant negative flows at the centrifugal compressor inlet are approximately 0.029 s (1/frequency) long. During these short periods, the centrifugal compressor would likely experience periodic surge events. However, if the reciprocating compressor speed is limited to below 15 Hz, the centrifugal compressor operation would be maintained stable. Clearly, using proper pulsation piping system design analysis, one can identify damaging operating speeds and design machine controls with speed exclusion region to achieve safe system operation.

On the other hand, for Case 3, the stable centrifugal compressor operating range is shifted to slightly above 18 Hz, as can be seen in Fig. 14. Here, minimum inlet flow velocities stay above the 1.7 kg/s surge limit on the 8000 rpm speed line, as long as the reciprocating compressor operates below 18 Hz. The periodic cycling of the centrifugal compressor's operating point can be plotted on its head-flow curve to visualize the impact of inlet pulsations on its performance and stability. For example, Fig. 16 shows the centrifugal compressor operating point variations (on the map) due to inlet flow pulsations when the reciprocating compressor is operating at 17 Hz. Although the centrifugal compressor's operating point fluctuates significantly on the constant speed line (from 2.1 kg/s to 3.8 kg/s), the compressor will not cross the surge line at this operating condition. However, it is still possible that the compressor may experience diffuser stall as this is common when operating near the surge line.

This wide operating point fluctuation is still not desirable as (1) the compressor operates a significant percentage of time away from its best efficiency point, and (2) any small operating change could move the compressor across the surge line. A reduction of less than 15% in flow, or increase of 10% in system suction pressure, would lead to compressor surge, which indicates a severely restricted plant operating range. Also, centrifugal compressor's isentropic efficiencies vary widely between 72% and 56%, with a time-averaged mean value of only 61%. Although a functional compression system solution was achieved, further piping pulsation and machine design optimization would be desired for this case.

6 Conclusions

The above examples demonstrate that by properly analyzing and designing the interconnecting piping between the compressors, utilizing pulsation attenuation devices, and matching the compressor's mass-flow rates, a satisfactory functional compression system design can be achieved for even the worst cases of mixed centrifugal and reciprocating compressor operation. Nonetheless, from the above examples, it is also apparent that even small analysis errors, design deviations, or machine mismatches can lead to a severely operational restricted (or even inoperable) compression system. Also, pulsation attenuation designs often lead to significant piping pressure losses. Utilizing analysis tools in the design process that can accurately model the transient fluid dynamics of the piping system, the pulsation attenuation devices, and the compressor machine behavior is critical to minimize piping pressure losses and to avoid potentially costly pulsation induced pipe or machine failures.

Acoustic analysis software that solves the linearized transient wave equations have been traditionally utilized for the piping resonance analysis of reciprocating compression systems. However, these solvers were found to be inadequate for the analysis of the pulsating flows in mixed centrifugal and reciprocating compression systems, as they do not account for nonlinear fluid effects. Also, as theses solvers do not model physical flow (just perturbations from mean flow), they cannot properly predict real compressor performance and system pressure losses. Especially station designs, where the compressor mass-flows and performances are mismatched, can lead to the machines continuously "hunting" for a stable operating point, resulting in global low frequency nonperiodic pressure transients in the piping system.

A fully transient one-dimensional Navier–Stokes equation solver for any complex system of interconnected pipes was developed and found to be an efficient and accurate tool to accurately predict flows, pulsation amplitudes, and frequencies in mixed compression systems. This solver serves as an engineering tool to avoid critical piping design and compressor matching mistakes early in the compression station design process. However, even the most accurate transient flow solver technology is only useful if the original compression station design and subsequent field operating conditions reasonably coincide, and if the pulsation analysis/design recommendations are closely implemented. Proper planning from the outset is imperative in this process.

Nomenclature

A = pipe cross-sectional area
C = Brun–Kurz number
H = head
J = mass moment of inertia
P = pressure
Q = volume flow
R = gas constant
T = temperature

V = volume
Z = compressibility
c = speed of sound
f = pipe friction
j = node number
k = pipe friction coefficient
m = Mach number
$\Delta\dot{m}$ = mass-flow pulsation
r = radius
t = time
u = local velocity
x, y = distance
z = piston position
• = isentropic coefficient
• = clearance volume
μ = viscosity
• = density
• = crank angle
• = coefficient
• = angular speed

Subscripts and Superscripts

d = discharge
i = intersection
int = null node and intersection
j = node number
n = number of nodes in reach
s = suction

References

[1] Abdel-Hamid, A. N., "Dynamic Response of a Centrifugal Blower to Periodic Flow Fluctuations," *ASME*, Paper No. 85-GT-195.
[2] Aust, N., 1988, *Ein Verfahren zur digitalen Simulation instationaerer Vorgaenge in Verdichteranlagen*, Diss U Bw, Hamburg.
[3] Baldwin, R. M., and Simmons, H. R., "Flow-Induced Vibration in Safety Relief Valves: Design and Troubleshooting Methods," ASME Paper No. 84-PVP-8.
[4] Bar, L. C., 1979, "The Unsteady Response of an Axial Flow Turbomachinery Rotor to Inlet Flow Distortions," MS thesis, Department of Aerospace Engineering, Pennsylvania State University.
[5] Blodgett, L. E., 1992, "Theoretical and Practical Design of Pulsation Damping Systems," Flow Meas. Instrum., **3**(3), pp. 203–208.
[6] Brun, K., Deffenbaugh, D. M., and Bowles, E. B., Jr., 2007, "Development of a Transient Fluid Dynamics Solver for Compression System Pulsation Analysis," Gas Machinery Conference, Dallas, TX.
[7] Durke, R. G., and McKee, R. J., "Identification of Pulsation Induced Orifice Metering Errors Including Gage Line Shift," *The American Society of Mechanical Engineers*.
[8] Fletcher, C. A. J., 1991, *Computational Techniques for Fluid Dynamics*, Vol. I, Springer-Verlag, Germany.
[9] Henderson, R. E., 1972, "The Unsteady Attenuation of an Axial Flow Turbomachine to an Upstream Disturbance," Ph.D. thesis, Department of Engineering, University of Cambridge, England.
[10] Ingard, U., and Singhla, V. K., 1974, "Sound in Turbulent Pipe Flow," J. Acoust. Soc. Am., **55**(3), pp. 535–538.
[11] Iwasaki, M., Ikeya, N., Marutani, Y., and Kitazawa, T., 1994, "Comparison of Turbocharger Performance Between Steady Flow and Pulsating Flow on Engines," *Proceedings of the SAE International Congress and Exposition*, Detroit, MI.
[12] Kinsler, L. E., Frey, A. R., Coppens, A. B., and Sanders, J. V., 2000, *Fundamentals of Acoustics*, Wiley, New York.
[13] Kurz, R., McKee, R., and Brun, K., "Pulsations in Centrifugal Compressor Installations," *ASME*, Paper No. GT2006-90700.
[14] Meyer, W., 1988, *Untersuchungen zum Einfluss von Einlaufdrallstoerungen auf das stationaere Betriebsverhalten von Turbostrahltriebwerken*, Diss U Bw, Muenchen.
[15] Shapiro, L., 1996, *Performance Formulas for Centrifugal Compressors*, Solar Turbines.
[16] Smalley, A. J., Jungbauer, D. E., and Harris, R. E., 1995, "Reciprocating Compressor Reliability Issues," *Proceedings of the Fourth Process Plant Reliability Conference*, Houston, TX.
[17] Sparks, C. R., 1983, "On the Transient Interaction of Centrifugal Compressors and Their Piping Systems," ASME Paper No. 83-GT-236.
[18] Szymko, S., Martinez-Botas, R. F., and Pullen, K. R., 2005, "Experimental Evaluation of Turbocharger Turbine Performance Under Pulsating Flow Conditions," ASME Paper No. GT2005-68878.
[19] Wachter, J., and Loehle, M., 1985, "Identifikation des dynamischen Uebertragungsverhaltens eines dreistufigen Radialverdichters bei saug- und druckseitiger Durchsatzvariation," VDI Bericht 572.2, pp. 365–379.
[20] Yocum, A. M., and Henderson, R. E., 1980, "The Effects of Some Design Parameters of an Isolated Rotor on Inlet Flow Distortions," ASME J. Eng. Power, **102**, pp. 178–186.
[21] Morini, M., Pinelli, M., and Venturini, M., 2007, "Development of a One-Dimensional Modular Dynamic Model for the Simulation of Surge in Compression Systems," ASME J. Turbomach., **129**(3), pp. 437–447.